Chemistry–A European Journal
Research Article
doi.org/10.1002/chem.202203468
Chemistry Europe
European Chemical Societies Publishing
www.chemeurj.org

Excited-State Dynamics in Borylated Arylisoquinoline Complexes in Solution and *in cellulo*

Tingxiang Yang,[a, b] Abha Valavalkar,[a, b] Antonio Romero-Arenas,[d] Anindita Dasgupta,[a, c] Patrick Then,[a, c] Avinash Chettri,[a, b] Christian Eggeling,[a, c, e, h] Abel Ros,*[d] Uwe Pischel,*[f] and Benjamin Dietzek-Ivanšić*[a, b, h]

Abstract: Two four-coordinate organoboron *N*,*C*-chelate complexes with different functional terminals on the PEG chains are studied with respect to their photophysical properties within human MCF-7 cells. Their excited-state properties are characterized by time-resolved pump-probe spectroscopy and fluorescence lifetime microscopy. The excited-state relaxation dynamics of the two complexes are similar when studied in DMSO. Aggregation of the complexes with the carboxylate terminal group is observed in water. When studying the light-driven excited-state dynamics of both complexes *in cellulo*, i.e., after being taken up into human MCF-7 cells, both complexes show different features depending on the nature of the anchoring PEG chains. The lifetime of a characteristic intramolecular charge-transfer state is significantly shorter when studied *in cellulo* (360 ± 170 ps) as compared to in DMSO (~960 ps) at 600 nm for the complexes with an amino group. However, the kinetics of the complexes with the carboxylate group are in line with those recorded in DMSO. On the other hand, the lifetimes of the fluorescent state are almost identical for both complexes *in cellulo.* These findings underline the importance to evaluate the excited-state properties of fluorophores in a complex biological environment in order to fully account for intra- and intermolecular effects governing the light-induced processes in functional dyes.

Introduction

Four-coordinate organoboron complexes are attractive luminophores for bioimaging, due to their highly emissive nature.[1] Consequently, the photophysical properties, for example absorption and emission spectra in solution, as well as when taken up into cells have been studied.[2] Spectroscopic studies revealed that the excited-state properties of such dyes are often determined by the presence of intramolecular charge-transfer (ICT) transitions, which are highly sensitive to the local environment of the fluorophore.[2b,3] A shortened ICT lifetime is present in polar solvents for some of the four-coordinate *N*,*C* organoboron complexes.[4] The polarity dependence of the ICT states causes a red-shifted and weakened emission as the polarity of the surrounding environment increases.[5] Solvent-induced aggregation also impacts the fluorescence of such organoboron compounds.[6]

Integrating an electron-donor-substituted arylisoquinoline as a chelate ligand, the ICT state, in which charge density is shifted to the isoquinoline part, constitutes an 'energy sink' and causes the large Stokes shifts beneficial for bioimaging.[7] Compounds following such design principles have been synthesized and studied for bioimaging by some of us:[7a,8] However, an in-depth time-resolved photophysical study of the

[a] *T. Yang, A. Valavalkar, A. Dasgupta, Dr. P. Then, A. Chettri, Prof. Dr. C. Eggeling, Prof. Dr. B. Dietzek-Ivanšić*
Leibniz Institute of Photonic Technology (Leibniz-IPHT)
Albert-Einstein-Straße 9, 07745 Jena (Germany)
E-mail: benjamin.dietzek@leibniz-ipht.de

[b] *T. Yang, A. Valavalkar, A. Chettri, Prof. Dr. B. Dietzek-Ivanšić*
Institute of Physical Chemistry
Friedrich Schiller University Jena
Helmholtzweg 4, 07743 Jena (Germany)

[c] *A. Dasgupta, Dr. P. Then, Prof. Dr. C. Eggeling*
Institute of Applied Optics and Biophysics
Friedrich Schiller University Jena
Helmholtzweg 4, 07743 Jena (Germany)

[d] *Dr. A. Romero-Arenas, Dr. A. Ros*
Institute for Chemical Research
CSIC-US and Innovation Centre in
Advanced Chemistry, ORFEO-CINQA
C/Américo Vespucio 49, 41092 Seville (Spain)
E-mail: abel.ros@liq.csic.es

[e] *Prof. Dr. C. Eggeling*
Member of the Leibniz Centre for Photonics in Infection Research (LPI), Jena (Germany)

[f] *Prof. Dr. U. Pischel*
CIQSO-Centre for Research in Sustainable Chemistry and Department of Chemistry
University of Huelva
Campus de El Carmen, s/n, 21071 Huelva (Spain)
E-mail: uwe.pischel@diq.uhu.es

[h] *Prof. Dr. C. Eggeling, Prof. Dr. B. Dietzek-Ivanšić*
Jena Center for Soft Matter (JCSM),
Philosophenweg 7, D-07743 Jena

Supporting information for this article is available on the WWW under https://doi.org/10.1002/chem.202203468

complexes in the environment of live human cells has not been reported so far.

In this contribution, we report on time-resolved spectroscopic studies of two borylated arylisoquinoline dyes. The complexes bear polyethylene glycol (PEG) chains with different functional terminal groups (–NH_2, –COOH, Scheme 1) to improve their water solubility.[9] This study presents a new viewpoint on spectroscopic-mechanistic research on organoboron fluorophores by observing the ultrafast light-induced dynamics when incorporated into live human cancer cells (MCF-7) and hence, exploring the effect of the dyes' interaction with the biological environment.

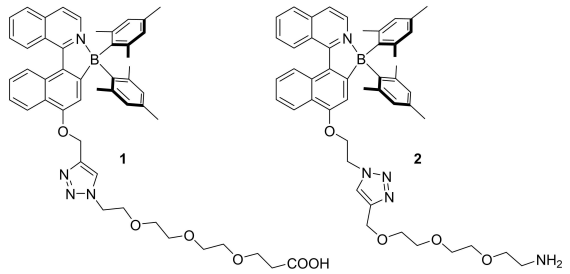

Scheme 1. Structures of the complexes **1** and **2** used in this work.

Results and Discussion

The dyes **1** and **2** were prepared in good yields (50–70%) by coupling of the corresponding alkyne (**6**)[7a] or azide derivatives (**7**) of the borylated arylisoquinolines with PEG-azide or PEG-alkyne derivatives, respectively, using a copper-catalyzed click reaction (see Scheme 2). The dyes were characterized by ^{1}H, ^{13}C, and ^{11}B NMR spectroscopy as well as by high-resolution mass spectrometry (see Supporting Information).

The discussion of the photophysical properties of the investigated organoboron dyes starts with the characterization of their steady-state absorption and emission. The absorption spectra of **1** and **2** show similar shapes (Figure 1) with maxima at 423 and 421 nm (Table 1) in DMSO, respectively, i.e., the PEG substituents do not alter the absorption and emission spectra of the fluorophore significantly.[10] The spectrum of **1** in water includes a small low-energy tail at ~480 nm, which is not present for **2**. Such solvent dependence can also be observed in the emission spectrum: in water, the emission spectrum of **1** becomes more structured with a maximum at 521 nm and a shoulder at 550–600 nm (Figure 1). These spectroscopic differences between **1** and **2** indicate the lower water solubility of **1** and its tendency to form aggregates.[11] The fluorescence quantum yields (Φ_{fluo}) of **1** and **2** in water are similar, 0.10 and 0.15, respectively. However, in DMSO the compounds exhibit significantly higher Φ_{fluo}, i.e., >0.9 (see Table 1). The difference

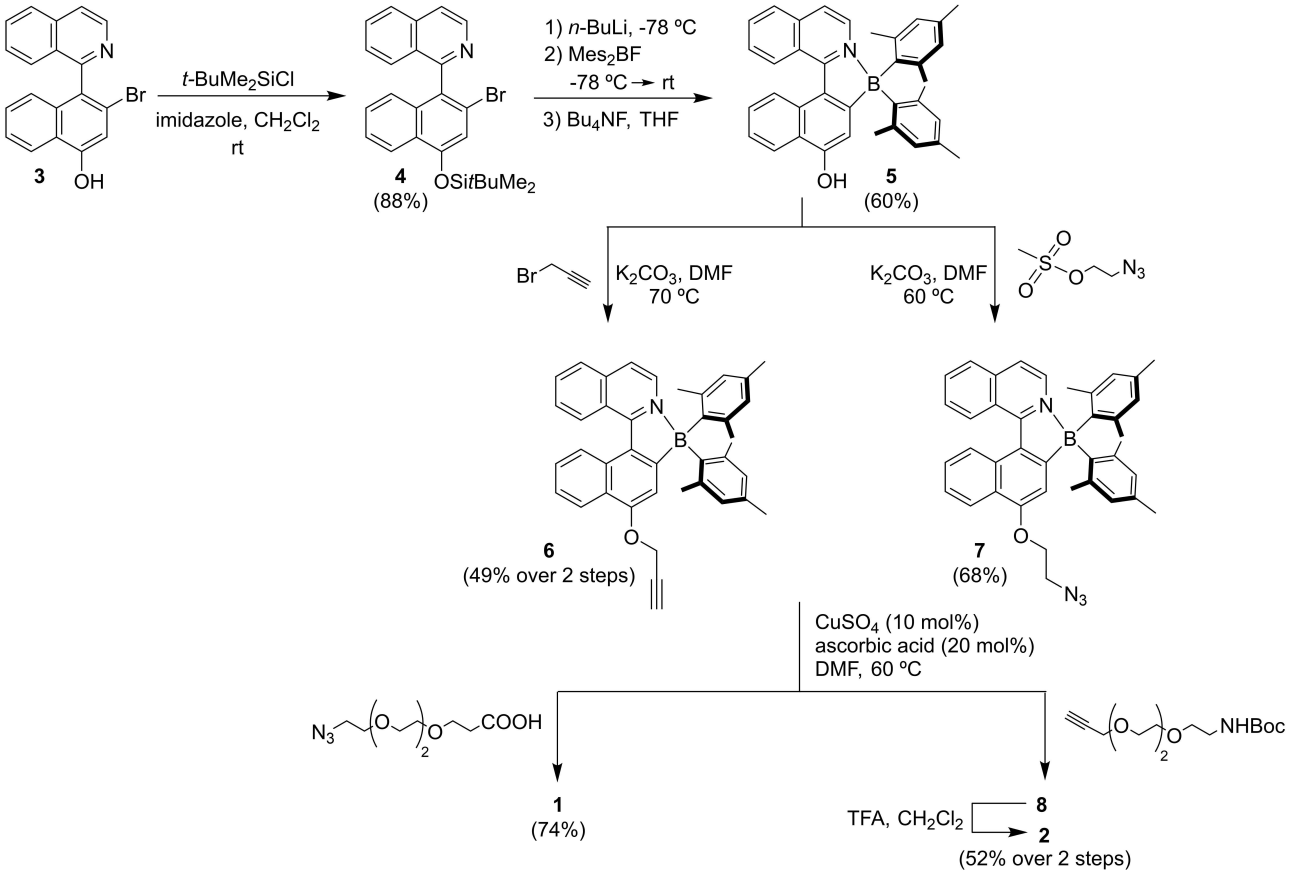

Scheme 2. Synthesis of the dyes **1** and **2**. For the compounds **3**–**6** see reference[7a].

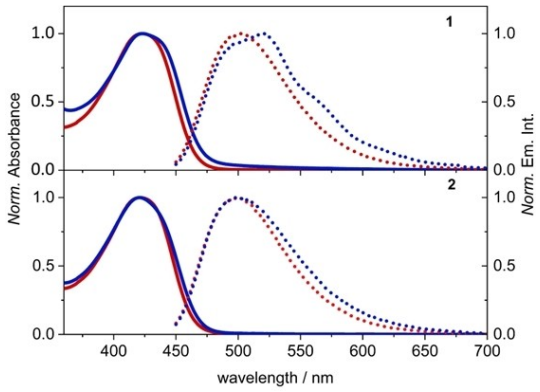

Figure 1. Normalized UV/vis absorption (solid line) and emission (dot line) spectra (λ_{ex} = 420 nm) of **1** (top) and **2** (bottom) in DMSO (red) and in water (containing 0.5 vol% DMSO, blue).

Φ_{fluo} in DMSO and water is also reflected in the fluorescence lifetime kinetics (Table 1 and Figure S2). Overall, the fluorescence lifetimes in water of **1** and **2** are much shorter than those recorded in DMSO. In addition a biexponential decay of the fluorescence of the compounds in water is observed. This might be an indication for aggregation taking place in water, significantly shortening the lifetime of the emission and rendering its decay more complex.

Transient Absorption (TA) Spectroscopy

Before considering *in cellulo* transient absorption kinetics of **1** and **2** in MCF-7 cells (see below), we recorded transient absorption data in solution. As both complexes show very similar transient absorption signatures in DMSO solution (Figure S3, S4 and S6), we will discuss the data obtained for **2** (Figure 2a and 2d for fs-transient absorption data). The data for **1** can be found in the Supporting Information (see Figure S3). The fs-transient absorption data show two positive ΔAbs bands at ca. 450 and 600 nm, while two minima are visible at ca. 420 and 510 nm (Figure 2a). The negative band at ca. 420 nm

Table 1. Photophysical properties of **1** and **2**.

Dye	Solvent	λ_{abs} [nm][a]	λ_{em} [nm][b]	Φ_{fluo} [c]	τ_{fluo} [ns][d]	A[f]	k_r [s^{-1}][g]
1	DMSO	423	501	0.93	7.1	100%	1.3×108
	water	423	521	0.10	0.5/1.5[e]	62%/38%	6×107
2	DMSO	421	497	0.99	7.2	100%	1.4×108
	water	421	498	0.15	0.3/1.9[e]	76%/ 24%	8×107

[a] Maximum of the steady-state absorption band. [b] Maximum of the emission band. [c] Absolute fluorescence quantum yield measured with an integrating sphere. [d] Fluorescence lifetime. [e] A bi-exponential decay of the respective signal is observed. [f] a_i is the amplitude of the corresponding fluorescence lifetime component, and A is the percentage weight of the amplitude, $A = a_i/(a_1 + a_2) \times 100\,\%$. [g] Radiative decay rate constant, $k_r = \Phi_{fluo}/\tau_{fluo}$.

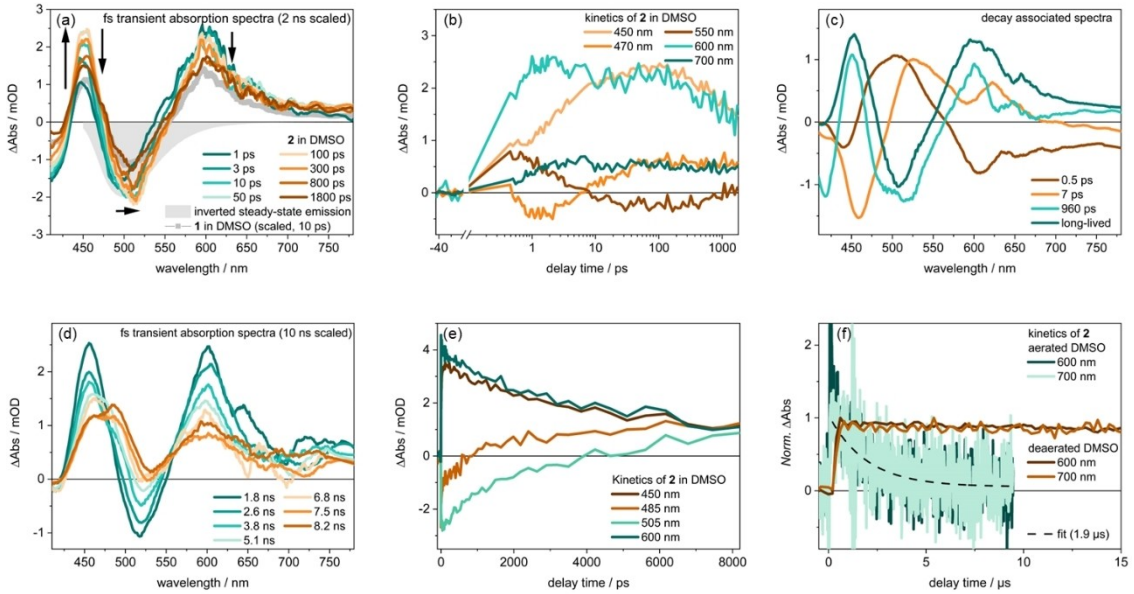

Figure 2. (a) fs-Transient absorption spectra of **2** in DMSO with λ_{ex} = 400 nm at different delay times as well as the transient absorption spectrum of **1** at 10 ps in grey; (b) Kinetic traces of selected wavelengths in the 2-ns time window; (c) Decay associated spectra of **2**. (d) Transient absorption spectra of **2** in DMSO in 10-ns time window; (e) Kinetic traces of **2** at 450, 485, 505 and 600 nm recorded in DMSO in 10/ns time window; (f) Kinetics of the decay at 600 and 700 nm for **2** in deaerated and aerated conditions. The spectra are smoothed by the Savitzky-Golary method to reduce the electronic noise (the original data are shown in Figure S3, S4, and S5). Concentration: 20 µM.

coincides with the inverted steady-state absorption spectrum and reflects the ground-state bleach (GSB). The negative band between 470–550 nm spectrally conincides with stimulated emission as seen from the inverted emission spectrum. During the first ca. 50 ps after photoexcitation, this negative differential absorption band shifts from 490 to 510 nm. At the same time the prominent excited-state absorption (ESA) band at the wavelength longer than 550 nm decreases, while differential absorption features at 450 nm and 700 nm increase (Figure 2b). The changes are highlighted in the decay-associated spectra (DAS) (Figure 2c), which are based on multi-exponential fitting of the experimental data. The time constants shown on DAS are determined by global fitting of the transient absorption data, i.e., the kinetic traces at all probe-wavelengths. The previously described spectral changes are associated with two decay components in the fit, characterized by time constants of 0.5 and 7 ps. We interpret the processes as a relaxation of the system from the Franck-Condon region (representing a locally excited state, LE) populating an ICT excited state. In the latter state electron density is shifted from the alkoxynaphthalene unit to the isoquinoline moiety of the complex.[7a] Similar assignments have been done for related *N,C* organoboron chelates.[7a,12] This ICT state is emissive, as indicated by the strong negative differential absorption band in the spectral region of the complex's fluorescence at 500–510 nm. Its decay appears to be biexponential with two very similarly shaped DAS in the kinetic modelling (see Figure 2c). While the shorter component, reflecting the decay of the ICT state, is associated with a characteristic time constant of 960 ps, the residual decay is too slow to be appropriately modelled from the fs-transient absorption data recorded on a 2 ns delay line. However, transient absorption data recorded on a 10-ns delay line reveal a 7.4 ns decay component during which the stimulated emission features disappear (see Figure S5), while a new ESA band at 485 nm forms (see Figure 2d, 2e and Figure S5). Thus, we associate the 7.4 ns process with ^{1}ICT→^{3}ICT intersystem crossing (ISC) and hence, quenching of the emission.[12] The formation of a triplet state is corroborated by the oxygen sensitivity of the transient, observed on the μs timescale (Figure 2f): the population of the long-lived state is effectively quenched under aerated conditions; the lifetime under deaerated condition is 15 μs, whereas it shortens to ca. 1.9 μs in aerated DMSO. To estimate the order of magnitude of the ISC quantum yield (Φ_{ISC}) from the transient absorption data we regard the transient absorption signal recorded after 7 μs. Considering the singlet ICT lifetime of 7.4 ns, the excited-state population remaining after 7 μs will be the population of the triplet state (see the Supporting Information for details). Taking into account the number of photons per pulse and the molecular absorption cross section as well as the experimentally observable GSB at 7 μs, we conclude that Φ_{ISC} is ca. 0.2 for **1** and 0.1 for **2**. This defines a conservative estimate for Φ_{ISC}. Taking into account the error margin for Φ_{fluo} and Φ_{ISC} (ca. 10–20% error), it remains clear that no other excited-state processes interfere in the decay of the ICT state, because both quantities add up to about 100%. The main excited-state pathways, discussed above, are summarized in Scheme 3.

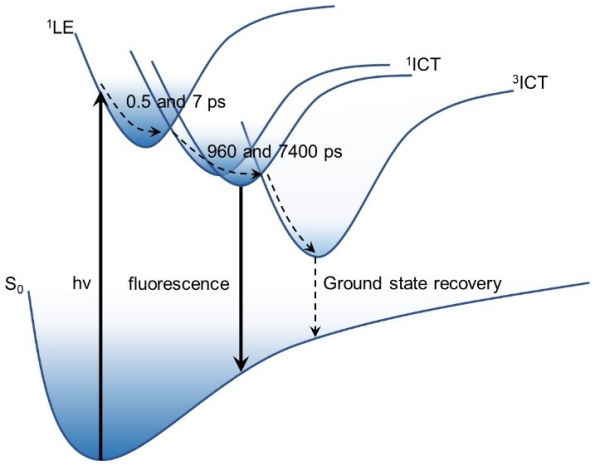

Scheme 3. Photophysical model for **2** in DMSO.

Intracellular Photophysics

To investigate the impact of the local environment on the excited state relaxation processes when **1** and **2** are taken up into human breast cancer cells, MCF-7 cells were dosed with 20 μM of either of the dyes. The uptake of **1** and **2** into MCF-7 cells was monitored by Lattice-SIM microscopy after a 3-h incubation period (Figure 3 and Figure S8). The compounds show effective permeability into the cells and are mainly localized in the cytoplasm. Similar observations were made for other four-coordinate organoboron complexes with the potential to be used in bioimaging.[7a,13] Figure 3 further indicates that

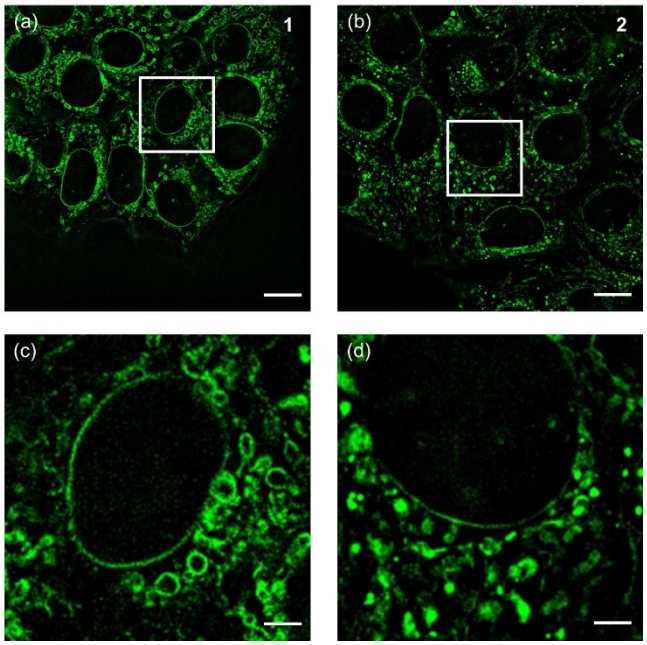

Figure 3. Cellular accumulation of **1** (a) and **2** (b), scale bar: 10 μm. (c) and (d) are the zoom-in images at the selected positions for **1** and **2**, respectively (scale bar: 2.5 μm). Representative Lattice-SIM images of live MCF-7 cells.

1 and **2** exhibit a tendency to bind to the nuclear membrane, as highlighted by the strong large ring-like central pattern in the Lattice-SIM images, which is slightly more pronounced for **1** compared to **2**. Apart from the nuclear membrane staining, the images disclose different cytosolic patterns for both compounds, suggesting that they bind to slightly different components within the cellular environment. **1** shows many roundish patterns, characteristic for staining of the membrane of cytosolic vesicles, whereas **2** elicits dotted patterns indicating staining of the matrix of such vesicle.

The fluorescence lifetimes of **1** and **2** *in cellulo* were obtained by fluorescence-lifetime imaging (FLIM). **1** and **2** feature a similar distribution of emission lifetime in the range of 4–8 ns and an average emission lifetime of ~6 ns (Figure 4). This *in cellulo* emission lifetime corresponds to the fluorescence lifetime of the dyes in DMSO (ca. 7 ± 0.2 ns), which indicates that the radiative pathways of **1** and **2** are not significantly affected by the local environment *in cellulo*. Noticeably, the emission lifetimes do not resemble those recorded in water, indicating that the dyes' tendency to aggregate in water is counterbalanced in the cellular environment,[7a,14] and hence, emission lifetimes resembling those of isolated **1** and **2** are observed.

To interrogate the ultrafast dynamics, i.e., with the higher lying electronic state of the excited-state potential energy surfaces of the dyes in MCF-7 cells, **1** and **2** were excited at 400 nm *in cellulo* and the photoinduced dynamics were studied at various probe wavelengths in the visible spectral range. This technique is rather singular and has been used for only few examples reported in the literature.[15] The data and insights that are obtained are of high value for dye design and provide a very detailed picture of the dyes' photophysics in the actual cellular environment. To check if the cells were damaged by the light-induced processes, trypan blue staining was used as a live/dead cells agent after each of the measurements. No significant number of cells stained by trypan blue was observed (Figure S15), reflecting the only marginal photocytotoxicity of the complexes under the experimental conditions used.

Figure 5 shows the transient absorption kinetics recorded from live MCF-7 cells dosed with **1** (first row) or **2** (second row). The third row in Figure 5 reports on control measurements, essentially showing the transient absorption background, which

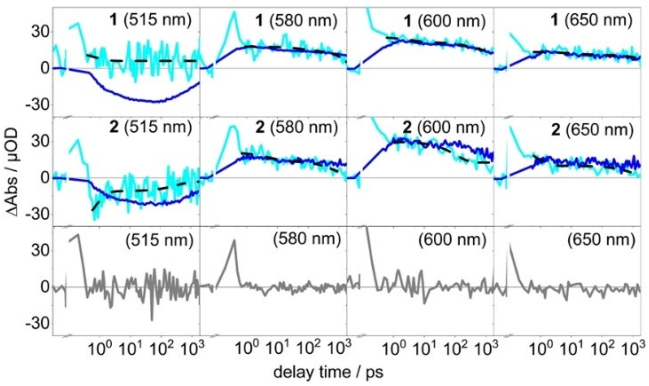

Figure 5. Kinetic traces of **1** (first row) and **2** (second row) at selected wavelengths were measured with live MCF-7 cells (cyan line), and recorded in DMSO (blue line). The dash black line is the fit data. The control experiments (only MCF-7 cells without complexes) are shown on the third row (grey line).

is obtained from live unstained MCF-7 (the small feature at pulse overlap stems from the coherent artifact).[16] The highest signal-to-noise ratio for the *in cellulo* transient absorption kinetics is obtained with a probe wavelength of 600 nm. This is in line with the transient absorption spectrum of **1** and **2** recorded in DMSO, which peaks at this wavelength. However, also at different probe wavelengths the kinetics can be resolved, i.e., probing at 580 nm as well as 650 nm yields positive differential absorption kinetics *in cellulo*. These experiments allowed for capturing excited-state absorption kinetics of the LE and ICT states (Figure 5). The kinetic traces of **1** are in good agreement with those recorded in DMSO at these three probe wavelengths, indicating that the overall nature of the LE state and ICT state is not impacted by the local environment provided by live MCF-7 cells in this particular example. On the contrary, differences are observed when comparing the transient absorption kinetics recorded for **2** at 600 nm *in cellulo* and in DMSO. The kinetics indicate that the sub-ns characteristic time constant reflecting the fast component of the decay of the emissive ICT state appears shortened from about 960 ps in DMSO to 360 ± 170 ps (Figure S13). The signal-to-noise ratio of the kinetics recorded at 650 nm is insufficient to conclude if the

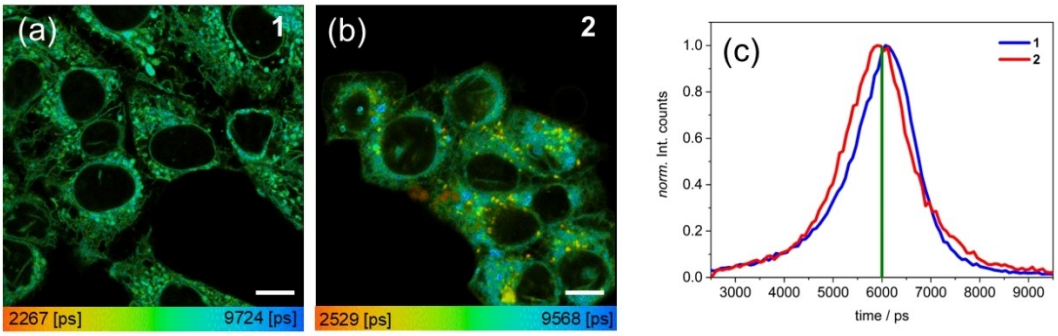

Figure 4. FLIM micrographs of **1** (a) and **2** (b), respectively (Scale bar: 5 μm). (c) Fluorescence lifetime distribution for **1** and **2**.

same observation can be made at this wavelength (see Figure S14). By probing the excited-state kinetics at 515 nm we expected to see also contributions from stimulated emission based on the transient absorption spectra recorded in DMSO. For **2** in live cells, slight indications for such a negative differential absorption signal are observed, while the low signal-to-noise ratio does not allow for such conclusions when studying **1** in MCF-7 cells.

The difference in the decay of the ICT state when comparing **1** and **2** (see deviations in the transient absorption kinetics measured *in cellulo* at 515 and 600 nm) provides an indication that the different local environments of the dyes in MCF-7 cells (i.e., **1** is located in the membrane of cytosolic vesicles, while **2** is found in the vesicle) lead to slightly different ICT stabilities and hence lifetimes. Apparently, only the higher lying electronic parts of the potential energy surface seem to be affected by the (slightly) different localization within the cells. The radiative lifetime, on the other hand, reflecting the time of ISC, which ultimately quenches the fluorescence of the complexes, remains the same for **1** and **2**.

Conclusion

In this contribution four-coordinate organoboron *N*,*C*-chelates were studied with respect to their excited-state relaxation pathways in solvents and when incorporated into human cancer cells (MCF-7). The different terminal groups (NH_2 or COOH) of the PEG chains, that were attached to the dyes, do not affect the excited-state relaxation pathways of the dyes when studied in DMSO. A slightly different distribution of the dyes within the MCF-7 cells was noted, which led to alterations of the decay kinetics of the emissive ICT state. Despite this observation, fluorescence lifetime imaging reveals the same distribution of emission lifetime for both dyes (which match the emission lifetimes of the dyes in DMSO). However, the fast relaxation component of the ICT state appears to be longer in **1** compared to **2** when both systems are taken up into MCF-7 cells. This indicates that the two PEG chains affect the localization of the dyes in cells, causing them to experience a distinct microenvironment, which in turn leads to slight differences in the slow structural relaxation of the emissive ICT state.

Experimental Section

The starting materials **3**–**6** (Scheme 2), 2-azidoethyl methanesulfonate, and the PEG-linkers were synthesized according to the procedures described in the literature.[7a,17]

Fluorescence lifetimes in solutions were measured with a Hamamatsu HPDTA streak camera. The excited wavelength was set at 400 nm with a repetition rate of 400 kHz. The response function is ca. 250 ps. Sample were measured in 1 cm quartz cuvettes.

Transient absorption spectra were obtained with a home-built setup.[18] 400 nm pump pulse of ca. 110 fs pulse duration with 500 Hz repetition rate and a white-light with 1 kHz repetition rate are focused on the sample position. The polarization between the pump and probe beam is set at the magic angle (ca. 54.7°). The solvent samples were measured in 1 cm quartz cuvettes.

For the *in cellulo* experiments, the single wavelength probes (515, 580, 600 and 650 nm) are employed instead of the white light. The cellular samples were measured in glass bottom μ-dishes. The MCF-7 cells were treated with final concentration of 20 μM of **1** and **2** in media. The MCF-7 cells were measured in 1 mL Hanks' balanced salt solution (HBSS). Following the measurements, the cells were treated with Trypan Blue solution and imaged by a combination of a Raspberry Pi camera and Carl Zeiss Axiovert 25 microscope with the objective EC Plan-Neofluar 10X/0.30M27 (Figure S15).

Nanosecond transient absorption spectroscopy was used to obtained the kinetics at long delay time. The pump pulse was set at 430 nm produced by Surelite Nd:YAG laser system with a pulse duration of 5 ns and a repetition rate of 10 Hz. The white-light probe is provided by a xenon arc lampand samples were measured in 1 cm quartz cuvettes. Oxygen-free solutions were prepared inglove box.

Fluorescence lifetime images were obtained from a custom Abberior Expert Line laser scanning STED microscope with 100× /1.4 oil immersion objective lens from Olympus. The MCF-7 cells were seeded on a glass coverslip with 20 μM concentration of each of the dyes. The cell samples were excited at 440 nm pulses with a repetition rate of 40 MHz.

Lattice-SIM images were acquired on a Zeiss Elyra 7 microscope equipped with a Plan-Apochromat 63X/1.4 Oil DIC M27 objective and a pco.edge sCMOS (version 4.2 CL HS) camera. The 405 nm laser was used to excite the dyes *in cellulo*.

Acknowledgements

This work was supported by the European Union (via the ITN LogicLab funded under the Horizon 2020 research and innovation program under the grant agreement No 813920). We thank Prof. Dr. Rainer Heintzmann and Dr. Benedict Diederich for providing BioLab facilities and supporting the image acquisition. The ELYRA 7 (used for producing Figure 3 and S8) was funded by the Free State of Thuringia with grant number 2019 FGI 0003 and supported by the Microverse Imaging Center (funded by the DFG under Germany Âs Excellence Strategy ®EXC 2051 ®Project-ID 390713860). We further acknowledge funding by the DFG (Project number 316213987 – SFB 1278, INST 1757/25-1 FUGG), the Free State of Thuringia (TAB, TMWWDG, AdvancedSTED/2018 FGI 0022; Advanced Flu-Spec/2020 FGI 0031), BMBF (Photonics Research Germany (FKZ; 3N15713/13N15717) integrated into the Leibniz Center for Photonics in Infection Research (LPI)) and the innovation program by the German BMWi (ZIM; project 16KN070934 / Lab-on-a-chip FCS-Easy). The Spanish *Ministerio de Ciencia e Innovación* (grants PID2020-119992GB-I00, PID2019-106358GB-C21, and PID2019-106358GB-C22), the *Consejo Superior de Investigaciones Científicas* (grant 202080I005 for A.R.), and the *Junta de Andalucía*/University of Huelva (grant UHU-202070) are thanked for financial support. We thank Dr. Z. Dom Nguez for assistance in the early stage of this project. Open Access funding enabled and organized by Projekt DEAL.

Conflict of Interest

The authors declare no conflict of interest.

Data Availability Statement

The data that support the findings of this study are available from the corresponding author upon reasonable request.

Keywords: excited-state relaxation · fluorescence · live cells · organoboron dyes · PEG chain

[1] a) R. Hecht, J. Kade, D. Schmidt, A. Nowak-Krol, *Chem. Eur. J.* **2017**, *23*, 11620–11628; b) M. V. Pinto, F. M. F. Santos, C. Barros, A. R. Ribeiro, U. Pischel, P. M. P. Gois, A. Fernandes, *Cells* **2021**, *10*.
[2] a) K. Liu, R. A. Lalancette, F. Jakle, *J. Am. Chem. Soc.* **2019**, *141*, 7453–7462; b) P. Li, H. Chan, S. L. Lai, M. Ng, M. Y. Chan, V. W. Yam, *Angew. Chem. Int. Ed. Engl.* **2019**, *58*, 9088–9094; c) M. Mas-Montoya, L. Usea, A. Espinosa Ferao, M. F. Montenegro, C. Ramirez de Arellano, A. Tarraga, J. N. Rodriguez-Lopez, D. Curiel, *J. Org. Chem.* **2016**, *81*, 3296–3302; d) F. M. F. Santos, Z. Dominguez, J. P. L. Fernandes, C. Parente Carvalho, D. Collado, E. Perez-Inestrosa, M. V. Pinto, A. Fernandes, J. F. Arteaga, U. Pischel, P. M. P. Gois, *Chem. Eur. J.* **2020**, *26*, 14064–14069.
[3] a) H. Gao, D. Xu, Y. Wang, C. Zhang, Y. Yang, X. Liu, A. Han, Y. Wang, *Dyes Pigm.* **2018**, *150*, 165–173; b) L. Jiang, Y. Wang, D. Tan, X. Chen, T. Ma, B. Zhang, D.-T. Yang, *Chem. Sci.* **2022**; c) Z. Zhang, P. Xue, P. Gong, G. Zhang, J. Peng, R. Lu, *J. Mater. Chem. C* **2014**, *2*, 9543–9551.
[4] S. K. Mellerup, G. Yousefalizadeh, S. Wang, K. G. Stamplecoskie, *J. Phys. Chem. A* **2018**, *122*, 9267–9274.
[5] a) M. Kollmannsberger, K. Rurack, U. Resch-Genger, J. Daub, *J. Phys. Chem. A* **1998**, *102*, 10211–10220; b) R. R. Maar, R. Zhang, D. G. Stephens, Z. Ding, J. B. Gilroy, *Angew. Chem. Int. Ed. Engl.* **2019**, *58*, 1052–1056.
[6] a) Z. Zhao, Z. Chang, B. He, B. Chen, C. Deng, P. Lu, H. Qiu, B. Z. Tang, *Chem. Eur. J.* **2013**, *19*, 11512–11517; b) S. Ito, M. Gon, K. Tanaka, Y. Chujo, *Natl. Sci. Rev.* **2021**, *8*, nwab049; c) M. Yamaguchi, S. Ito, A. Hirose, K. Tanaka, Y. Chujo, *Mater. Chem. Front.* **2017**, *1*, 1573–1579.
[7] a) V. F. Pais, M. M. Alcaide, R. Lopez-Rodriguez, D. Collado, F. Najera, E. Perez-Inestrosa, E. Alvarez, J. M. Lassaletta, R. Fernandez, A. Ros, U. Pischel, *Chem. Eur. J.* **2015**, *21*, 15369–15376; b) Z. Dominguez, R. Lopez-Rodriguez, E. Alvarez, S. Abbate, G. Longhi, U. Pischel, A. Ros, *Chem. Eur. J.* **2018**, *24*, 12660–12668.
[8] Z. Dominguez, V. F. Pais, D. Collado, P. Vazquez-Dominguez, F. N. Albendin, E. Perez-Inestrosa, A. Ros, U. Pischel, *J. Org. Chem.* **2019**, *84*, 13384–13393.
[9] a) H. Yang, J. J. Morris, S. T. Lopina, *J. Colloid Interface Sci.* **2004**, *273*, 148–154; b) Q. Song, S. Goia, J. Yang, S. C. L. Hall, M. Staniforth, V. G. Stavros, S. Perrier, *J. Am. Chem. Soc.* **2021**, *143*, 382–389; c) A. W. Bosman, H. M. Janssen, E. W. Meijer, *Chem. Rev.* **1999**, 1665–1688.
[10] F. M. Santos, J. N. Rosa, N. R. Candeias, C. P. Carvalho, A. I. Matos, A. E. Ventura, H. F. Florindo, L. C. Silva, U. Pischel, P. M. Gois, *Chem. Eur. J.* **2016**, *22*, 1631–1637.
[11] a) K. Kumar, J. Hiller, M. Bender, S. Nosrati, Q. Liu, M. Edelmann, S. Maier, T. Rammler, F. Wackenhut, A. J. Meixner, K. Braun, U. H. F. Bunz, M. Scheele, *ACS Nano* **2021**, *15*, 480–488; b) S. Nath, H. Pal, D. K. Palit, Avinash, V. Sapre, J. P. Mittal, *J. Phys. Chem. B* **1998**, 10158–10164; c) A. Nagai, J. Miyake, K. Kokado, Y. Nagata, Y. Chujo, *J. Am. Chem. Soc.* **2008**, *130*, 15276–15278.
[12] F. Bosca, M. C. Cuquerella, V. F. Pais, A. Ros, U. Pischel, *ChemPhotoChem* **2018**, *2*, 34–41.
[13] V. F. Pais, P. Ramirez-Lopez, A. Romero-Arenas, D. Collado, F. Najera, E. Perez-Inestrosa, R. Fernandez, J. M. Lassaletta, A. Ros, U. Pischel, *J. Org. Chem.* **2016**, *81*, 9605–9611.
[14] a) J. Rumin, H. Bonnefond, B. Saint-Jean, C. Rouxel, A. Sciandra, O. Bernard, J. P. Cadoret, G. Bougaran, *Biotechnol. Biofuels* **2015**, *8*, 42; b) A. Ray, S. Das, N. Chattopadhyay, *ACS Omega* **2019**, *4*, 15–24.
[15] a) K. R. A. Schneider, A. Chettri, H. D. Cole, K. Reglinski, J. Bruckmann, J. A. Roque, 3rd, A. Stumper, D. Nauroozi, S. Schmid, C. B. Lagerholm, S. Rau, P. Bauerle, C. Eggeling, C. G. Cameron, S. A. McFarland, B. Dietzek, *Chem. Eur. J.* **2020**, *26*, 14844–14851; b) T. Yang, A. Chettri, B. Radwan, E. Matuszyk, M. Baranska, B. Dietzek, *Chem. Commun.* **2021**, *57*, 6392–6395; c) B. M. Aveline, R. M. Sattler, R. W. Redmond, *Photochem. Photobiol.* **1998**, *68*, 51–62.
[16] B. Dietzek, T. Pascher, V. Sundström, A. Yartsev, *Laser Phys. Lett.* **2006**, *4*, 38–43.
[17] a) S. T. G. Street, D. N. Chin, G. J. Hollingworth, M. Berry, J. C. Morales, M. C. Galan, *Chem. Eur. J.* **2017**, *23*, 6953–6958; b) L. S. Wong, S. J. Janusz, S. Sun, G. J. Leggett, J. Micklefield, *Chem. Eur. J.* **2010**, *16*, 12234–12243; c) T. Anabuki, M. Tsukahara, H. Matsuura, K. Takahashi, *Biosci. Biotechnol. Biochem.* **2016**, *80*, 432–439.
[18] R. Siebert, D. Akimov, M. Schmitt, A. Winter, U. S. Schubert, B. Dietzek, J. Popp, *ChemPhysChem* **2009**, *10*, 910–919.

Manuscript received: November 8, 2022
Accepted manuscript online: December 7, 2022
Version of record online: February 14, 2023